Progress In Electromagnetics Research C, Vol. 72, 43–54, 2017

W-Band SIW Power Combiner/Divider Based on the Antipodal Fin-Line SIW-RW Transition and Longitudinal-Slot Coupling Techniques

Zhenbing Li, Jian Li, Yongjun Huang*, and Guangjun Wen

Abstract—In this paper, a novel W-band substrate integrated waveguide (SIW) power combiner/divider is analyzed theoretically and demonstrated experimentally/numerically, based on the antipodal fin-line SIW-rectangular waveguide (SIW-RW) transition and longitudinal slot coupling techniques. This antipodal fin-line SIW-RW transition can work at the frequency band of 86.4 GHz–106.1 GHz with return loss larger than 15 dB and inserting loss less than 2 dB. By combining the antipodal fin-line SIW-RW into the four-way longitudinal-slot SIW coupling structure, a novel back-to-back power dividing/combining system is achieved, which can operate at the frequency band of 92.8 GHz–93.8 GHz with return loss more than 10 dB and insertion loss less than 3.9 dB. Such a design can be used in future for spatial power amplifier applications.

1. INTRODUCTION

Recently, with the developments of communication system in military and civil areas, high-power amplifier as an indispensable component has been a technique barrier, and researchers across the world have focused on this issue to propose various solutions [1]. The developed designs include electron tubes [2], solid state power devices [3], and spatial power combing techniques [4]. In view of these designs, the traditional electron tubes can work on very high power level but are limited by the fabrication technique, complex system, and large size and weight. Based on the well-developed semiconductor technology, the solid-state power devices have been the main high-power amplifier components due to high-power capacity, high frequency and high efficiency advantages. However, solid-state power devices still suffer from the complex control system for the heat radiation, impedance matching, etc.

To solve these problems, researchers developed the power combing technique by using more than one method to achieve the expected targets [5, 6]. Especially, based on the metallic waveguide, the new spatial power combing method [7, 8] is considered as the desired solution due to various advantages, such as high combing efficiency, good heat transfer, wide operating frequency band, and low system loss. Moreover, the quite recently proposed substrate integrated waveguide (SIW) [9] can further reduce the 3-D dimensional spatial size [10]. Also, SIW can be fabricated by the traditional printed circuit board (PCB) and low-temperature co-fired ceramic (LTCC) techniques, and can be integrated and transited to standard rectangular waveguides, microstrips, or integrated circuits.

In the past few years, various SIW power combing/dividing designs have been reported [11–20], since the realization of SIW [9]. For examples, Germain et al. firstly proposed two kinds of basic Y-shaped and T-shaped two-way power dividers which show the relative bandwidths of 25.2% and 10.2%, respectively [11]. Based on the Y-shaped two-way power divider unit, Hao et al. designed a 16-way SIW power divider with a return loss larger than 15 dB and isolations larger than 14.5 dB

Received 7 January 2017, Accepted 8 February 2017, Scheduled 28 February 2017
* Corresponding author: Yongjun Huang (yongjunh@uestc.edu.cn).
The authors are with the Centre for RFIC and System Technology, School of Communication and Information Engineering, University of Electronic Science and Technology of China, Chengdu 611731, China.

within the operating band of 10.25 to 12 GHz [12]. Then, Liu et al. reported several Ku-band compact power combiners/dividers based on the size reduced half-mode SIW HMSIW technique [13], and Jin and Wen designed a four-way power combiner/divider by integrating the microstrip lines to the open wall of the HMSIW [14]. Moreover, by using the multi-mode interference imaging theory, Yang et al. realized a K-band 6-way multi-mode SIW (MMSIW) power combiner/divider [15]. Quite recently, some other researchers reported high-performance power combiners/dividers based on the various realization methods as well [16–20].

On the other hand, the W-band of the microwave part of electromagnetic spectrum ranging from 75 to 110 GHz (wavelength: 2.7–4 mm) has very important potential applications, e.g., satellite communications, millimeter-wave radar research, military radar targeting and tracking, and some other non-military applications. For the power combining techniques operating at W-band, however, only few works have been reported and numerically demonstrated [21–25].

In this paper, we experimentally/numerically propose and demonstrate a novel W-band substrate integrated waveguide (SIW) power combiner/divider, based on the antipodal fin-line SIW-rectangular waveguide (SIW-RW) transition and longitudinal slot coupling techniques. This antipodal fin-line SIW-RW transition can work at a wide frequency band with large return loss and small inserting loss. By combining the antipodal fin-line SIW-RW into the four-way longitudinal-slot SIW coupling structure, a novel back-to-back power dividing/combining system is achieved, which can operate at the frequency band of 92.8–93.8 GHz with return loss of more than 10 dB and insertion loss of less than −3.9 dB. The proposed structure possesses simpler configuration with only two function layers than the multilayer structures [17, 20] and exhibits similar working bandwidth but with lower inserting loss performance than the reported W-band power divider/combiner [24]. Such a design can be used in future for the spatial power amplifier applications.

2. DESIGN OF THE FOUR-WAY LONGITUDINAL-SLOT SIW COUPLING STRUCTURE

2.1. Theoretical Analysis

Based on the previously developed theoretical analysis on the longitudinal-slot in traditional metallic rectangular waveguide [26–28] and the recently realized Ka-band power amplifier based on the slot waveguide power comber/divider [29], we know that the combing/dividing of electromagnetic energy is mainly achieved by the mutual couplings between the slots and the microstrips laid on the slots. When there are more than one combing/dividing paths in the coupling system, the reflection generated by each slot will be overlapped at the input/output port and finally affect the performance of the coupling and combiner/divider. Moreover, the impedance matching is a key issue when we try to realize the broadband power comber/divider. Therefore, we need optimize the positions and sizes of the slots and the lengths of the microstrips. However, it will be a time-consuming task if we directly optimize the design by electromagnetic simulation software. Here we first analyze the equivalent circuit model of the four-way longitudinal-slot SIW coupling structure and then perform the numerical optimizations to save the design period.

As shown in Fig. 1, the designed W-band SIW power combiner/divider is composed of an antipodal fin-line SIW-RW transition and four longitudinal-slot coupling structures. The antipodal fin-line SIW-RW transition will be discussed later, and here we first focus on the four-way longitudinal-slot coupling structure. To apply the theoretical analysis on the longitudinal-slot for traditional metallic rectangular waveguide to our designed SIW structure, we need firstly determine the effective width of the SIW. After we get the right effective width, the overall equivalent circuit model can be found in Fig. 1(a) based on the dielectric filled rectangular waveguide theory [26–28]. $Y_i = G_i + jB_i$ $(i = 1, 2, 3, 4)$ is the equivalent admittance of the rectangular slot to microstrip coupling unit. L_0 is the distance of the first rectangular slot to the equivalent shorted terminal, Y_0 the characteristic admittance of TE10 mode of the SIW, and L_i $(i = 1, 2, 3)$ the distance between two adjacent coupling units. Therefore, we can obtain the equivalent admittance for each reference plane shown in Fig. 1(a) as

$$Y_1 = (G_1 + jB_1) + jY_0 \tan(\beta L_0), \quad Y_i = (G_i + jB_i) + Y_0 \frac{Y_{i-1} + jY_0 \tan(\beta L_{i-1})}{Y_0 + jY_{i-1} \tan(\beta L_{i-1})}, \quad i = 2, 3, 4 \qquad (1)$$

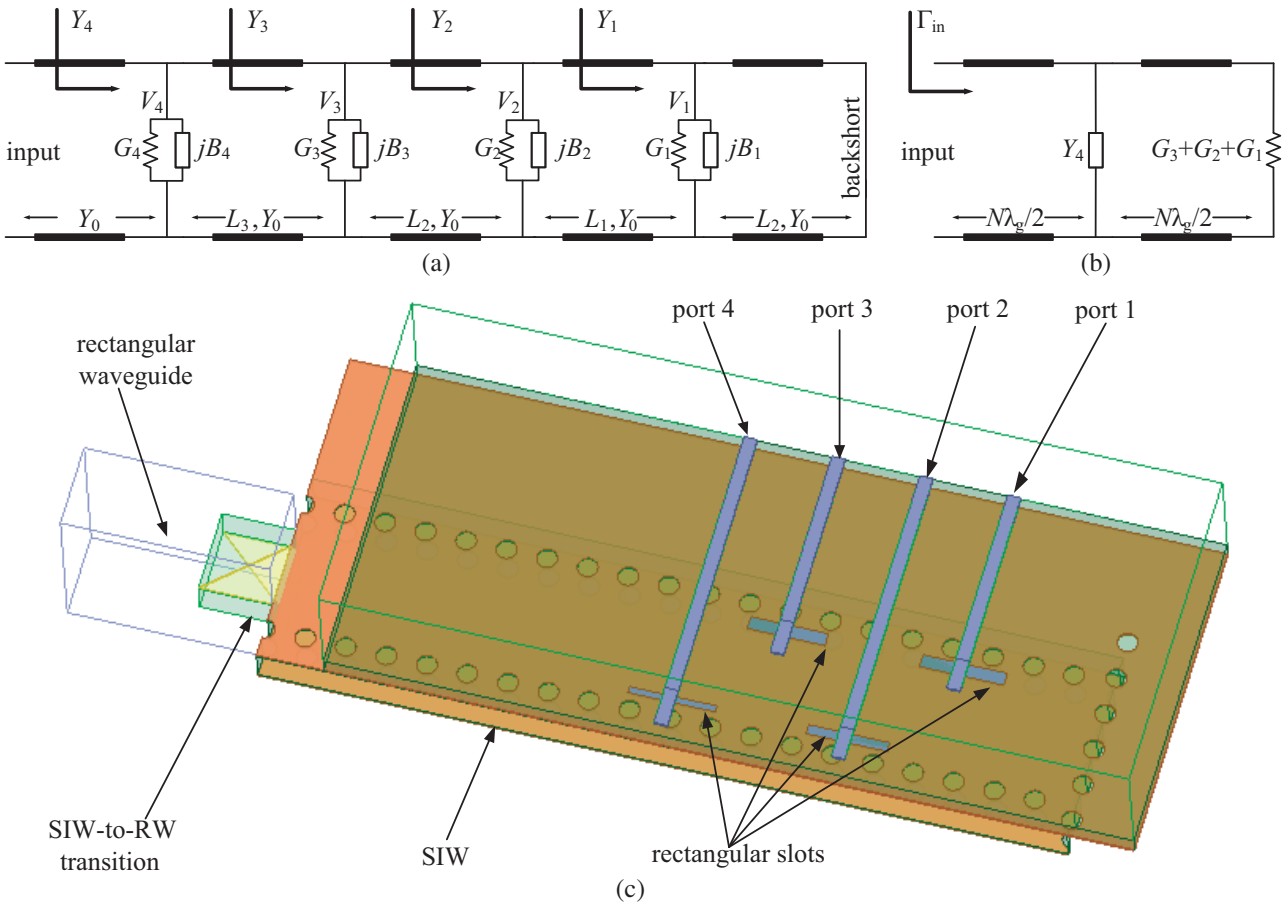

Figure 1. Designed W-band SIW power combiner/divider based on the antipodal fin-line SIW-RW transition and longitudinal-slot coupling techniques. (a) Equivalent circuit of the longitudinal-slot four-way SIW-RW coupling structure, (b) simplified equivalent circuit of the coupling structure, and (c) schematic representation of the full SIW power combiner/divider.

where $\beta = 2\pi/\lambda_g$. When we set the distance between the shorted terminal and the first slot as $L_0 = 3\lambda_g/4$, the equivalent admittance for the first slot should be $Y_1 = G_1 + jB_1$. Then the following distances keep constant (namely $L_1 = L_2 = L_3 = N\lambda_g/2$, $N = 1, 2, 3$), and so the magnitudes of all the output ports have the same level ideally [30]. And now the fourth equivalent admittance should be

$$Y_4 = (G_4 + jB_4) + (G_3 + jB_3) + (G_2 + jB_2) + (G_1 + jB_1) = \sum_{i=1}^{4}(G_i + jB_i) \tag{2}$$

Moreover, the coupling efficiency can achieve the maximum value when the resonance appears for the rectangular slot to microstrip coupling structure ($jB_i = 0$), and the power for each slot is

$$P_i = V_i^2 G_i/2 \tag{3}$$

and satisfies the relation

$$P_{in} = \sum_{i=1}^{4} P_i = \sum_{i=1}^{4} V_i^2 G_i/2 \tag{4}$$

So the equivalent admittance for the third coupling unit is

$$Y_3 = \sum_{i=1}^{3} G_i, \tag{5}$$

and we can get the simplified equivalent circuit model as shown in Fig. 1(b). Finally, the reflection of the input port is

$$\Gamma_{in}(\omega) = \frac{Y_0(\omega) - \sum_{i=1}^{4} G_i(\omega)}{Y_0(\omega) + \sum_{i=1}^{4} G_i(\omega)} \tag{6}$$

From Eq. (6) we know that to minimize the reflection the following relation should be achieved

$$Y_0(\omega) = \sum_{i=1}^{4} G_i(\omega) \tag{7}$$

Based on the above theoretical analysis, the term $V_i^2 G_i$ should be the same to keep equal power level for each output port. Therefore, we need carefully optimize the positions and sizes for the slots to achieve the previously analyzed targets.

2.2. Numerical Optimization

Now we start to numerically optimize the positions and sizes of the slots for the four-way coupling structure. Also, to save the optimize time, we consider the SIW as the dielectric filled rectangular

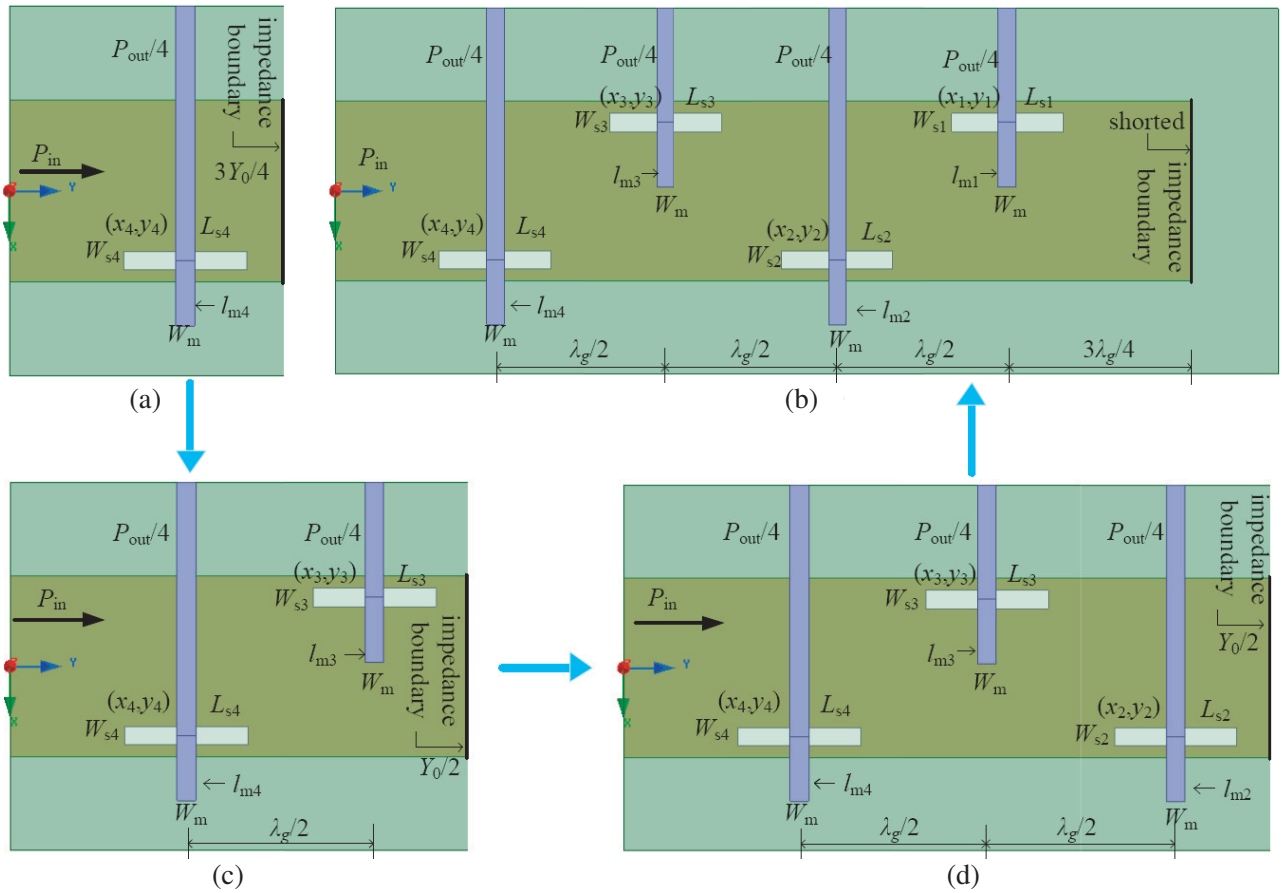

Figure 2. Design and optimization flow of the longitudinal-slot four-way coupling structure with structural parameter definitions. (a) The forth coupling unit, (b) the forth and third coupling units, (c) the second to forth coupling units, and (d) full coupling structure.

waveguide with the same effective width. Firstly, we design the slot to microstrip coupling unit as shown in Fig. 2. The structural parameters shown in Fig. 2 can be optimized in terms of the path number and port power dividing ratio. Then we optimize the structural parameters for each unit step-by-step as shown in Fig. 2: (1) the equivalent admittance Y_0 should be firstly determined based on the effective width and height of the dielectric filled waveguide. (2) For the fourth coupling unit, the theoretical equivalent admittance should be $3Y_0/4$, and the output power of the fourth unit should be $P_{in}/4$. (3) For the third coupling unit, the theoretical equivalent admittance should be $Y_0/2$, and the output power of the fourth unit should be $P_{in}/4$. (4) For the second coupling unit, the theoretical equivalent admittance should be $Y_0/4$, and the output power of the fourth unit should be $P_{in}/4$. (5) For the first coupling unit, the theoretical equivalent admittance should be zero, and the output power of the fourth unit should be $P_{in}/4$.

After the above-mentioned numerical optimization procedure, we obtain the initial structural parameters for the dielectric filed rectangular coupling system. Now we change back to the real longitudinal-slot SIW coupling structure as shown in Fig. 1(c). For the SIW coupling structure,a 0.508 mm Rogers RT/duriod 5880 dielectric substrate is used, and the dielectric constant is 2.2 and loss tangent 0.009 (measured at 100 GHz [31]). The radius of the hole is 0.15 mm, the distance between adjacent two holes 0.6 mm, and the distance between the two column holes 2.1 mm (namely the width of the SIW is 2.1 mm). Finally, the overall structural parameters are optimized by HFSS and concluded in Table 1. Here width W_m of all the four microstrip lines is 0.2 mm, and (x_i, y_i) stands for the positions of the slot related to the global coordinate system as shown in Fig. 1(c). In simulations and optimizations, the metallic surface roughness is considered by using the finite conductivity boundary with Huary model in HFSS.

The optimized results of the four-way longitudinal-slot SIW coupling structure can be found in Fig. 3, which shows that the inserting loss for each output port is about 7.85 dB$\pm$0.1 dB in the frequency range of 91.8 GHz–92.8 GHz. And the return loss for the whole simulation frequency band is below 15 dB. From the phase-frequency curve shown in Fig. 3(b), the differences among these four output ports is within 10 deg. Therefore, these results show that the optimized four-way longitudinal-slot SIW coupling structure has considerable magnitude-phase coherence.

Table 1. Optimized structural parameters of the longitudinal-slot SIW coupling structure (unit: mm).

x_1	y_1	W_{s1}	L_{s1}	l_{m1}	x_2	y_2	W_{s2}	L_{s2}	l_{m2}
−0.84	15.225	0.2	1.25	0.5	0.665	13.95	0.15	1.2	0.5
x_3	y_3	W_{s3}	L_{s3}	l_{m3}	x_4	y_4	W_{s4}	L_{s4}	l_{m4}
−0.84	12.675	0.2	1.15	0.54	0.69	11.3	0.1	1.3	0.59

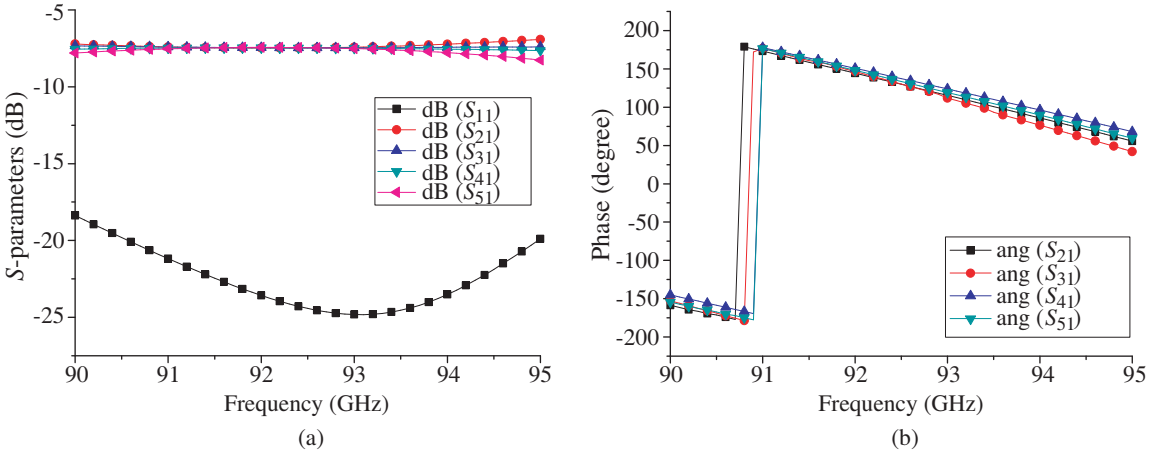

Figure 3. Numerical results of the designed longitudinal-slot four-way coupling structure. (a) Magnitude-frequency curves, and (b) phase-frequency curves.

To check the performance of the four-way power combiner/divider based on the longitudinal-slot SIW coupling structure, we further connect another four-way combiner to the divider as a back-to-back combiner/divider configuration as shown in Figs. 4(a) and (b). This method can effectively reduce the requirements for the further experimental measurements. Here we discuss two types of back-to-back configurations, the symmetric type and anti-symmetric type as shown in Figs. 4(a) and (b), respectively. From the numerical simulated electrical field distributions for these two types of power combiner/dividers, the anti-symmetric type has better energy coupling and transmitting performance than the symmetric type. Also, as shown in Figs. 4(e) and (f), the simulated transmission and reflection properties for the two types of power combiner/dividers further confirm the conclusion. Specially, the inserting loss and return loss of the anti-symmetric type power combiner/divider are about 3.3 dB and larger than 25.5 dB in the frequency range of 90 GHz–95 GHz. Therefore, we will choose the anti-symmetric type power combiner/divider for the experimental demonstrations.

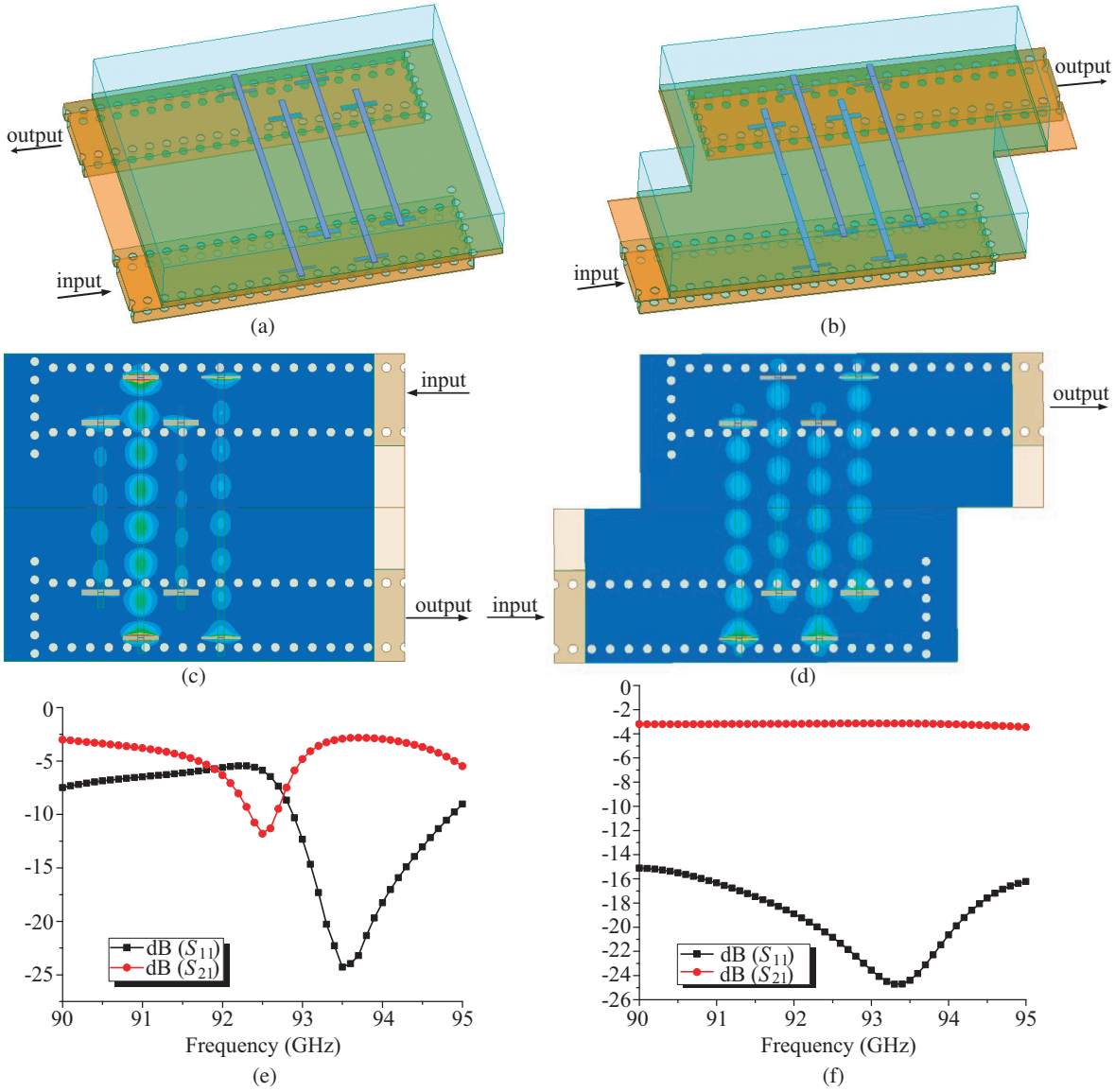

Figure 4. Designed two kinds of back-to-back SIW-RW four-way coupling structures. (a) Symmetric back-to-back configuration, (b) anti-symmetric back-to-back configuration, (c) electrical field distributions of the symmetric configuration, (d) electrical field distributions of the anti-symmetric configuration, (e) numerical results of the symmetric configuration, and (f) numerical results of the anti-symmetric configuration.

3. DESIGN AND DEMONSTRATION OF THE ANTIPODAL FIN-LINE SIW-RW TRANSITION

Now, we design the SIW-RW transition based on the well-developed antipodal fin-line technique [32]. For our designed SIW power combiner/divider, the operating frequency range is 75–110 GHz; the test waveguide is WR-10 (2.54 mm × 1.27 mm); the thickness of the RT/Duroid 5880 is 0.508 mm. Therefore, here we choose two kinds of the transition configurations. One is the cosine square line transition, and the other is the straight-line transition as shown in Fig. 5. Both antipodal fin-line configurations printed on opposite sides of the substrate are connected to the top and bottom conductors of the SIW directly, and then inserted into the E-plane of the standard RW. The antipodal fin-lines act as an antipodal dipole antenna and are excited by the SIW. The E-plane radiation of the antipodal dipole is along the E-plane of the RW. In that case, the transition can work well with low return loss and insertion loss.

Due to the similar configurations for the two structures, the cross-sectional E-field distributions for one of the proposed antipodal fin-line SIW-RW transitions are shown in Fig. 5(c). It can be seen that the x-polarized electric fields of TE10 mode of the RW can be converted smoothly to the z-polarized electric fields of the SIW. By performing the HFSS optimizations, the structural parameters for these two transitions are obtained as concluded in Table 2, and the transmission and reflection properties can

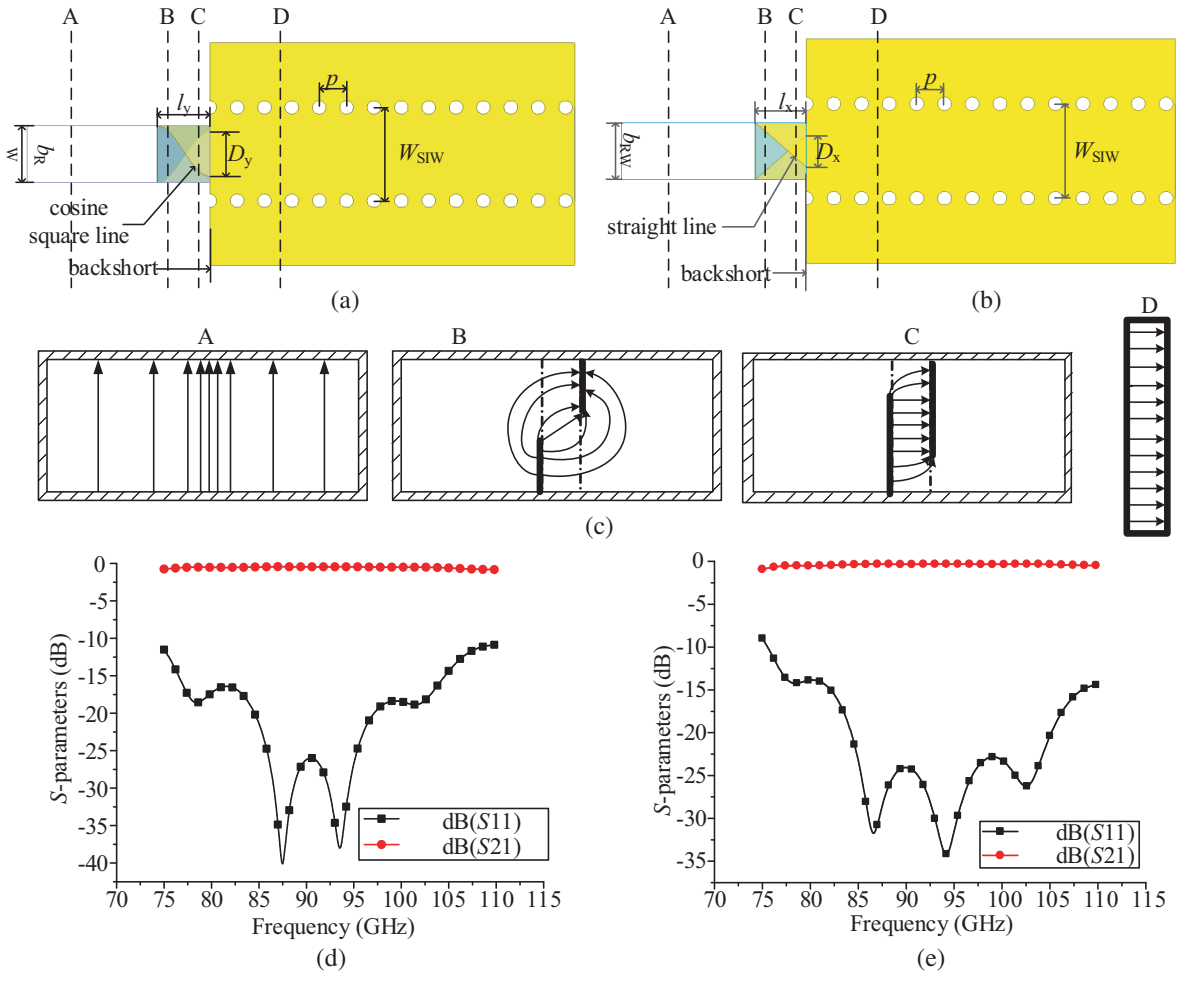

Figure 5. Designed two kinds of antipodal fin-line SIW-RW transitions. (a) Cosine square line configuration, (b) straight line configuration, (c) the cross-sectional E-field distributions for the transition, (d) numerical results of cosine square line SIW-RW transition, and (e) numerical results of straight line SIW-RW transition.

be found in Figs. 5(d) and (e), respectively. From the simulated transmission and reflection properties, we know that both transitions achieve the good electromagnetic transmitting abilities with inserting loss of below 1.0 dB and return loss of larger than 15 dB in the simulating frequency range. Comparing these two transitions, we can see that the straight-line transition has better performances with larger return loss and more flat inserting loss properties. Therefore, next we choose the straight-line transition as the main antipodal fin-line SIW-RW transition for further experimental demonstrations.

Moreover, because W-band devices have very small size compared with low frequency waveguide components, the fabrications tolerance will highly affect the performances of the transitions. And most of the right angles shown in Fig. 5(b) will be transferred to kind of chamfer edge as shown in Fig. 6(a). So we need numerically demonstrate the effects of the chamfer edge on the performances of the straight-line transition. As shown in Fig. 6(a), an additional parameter v is added to see the transmission and reflection changing properties when altering the value of v. From the simulated results as shown in Fig. 6(c), when the parameter v is set as 0.1 mm, the straight-line transition has better return loss properties.

Therefore, based on the above discussion, we design a back-to-back configuration as shown in

Table 2. Optimized structural parameters for the two antipodal fin-line SIW-RW transitions (unit: mm).

(a)	W_{SIW}	h	p	d	L_y	D_x
	2.1	0.508	0.6	0.3	1.25	0.45
(b)	W_{SIW}	h	p	d	L_x	D_x
	2.1	0.508	0.6	0.3	1.1	0.7

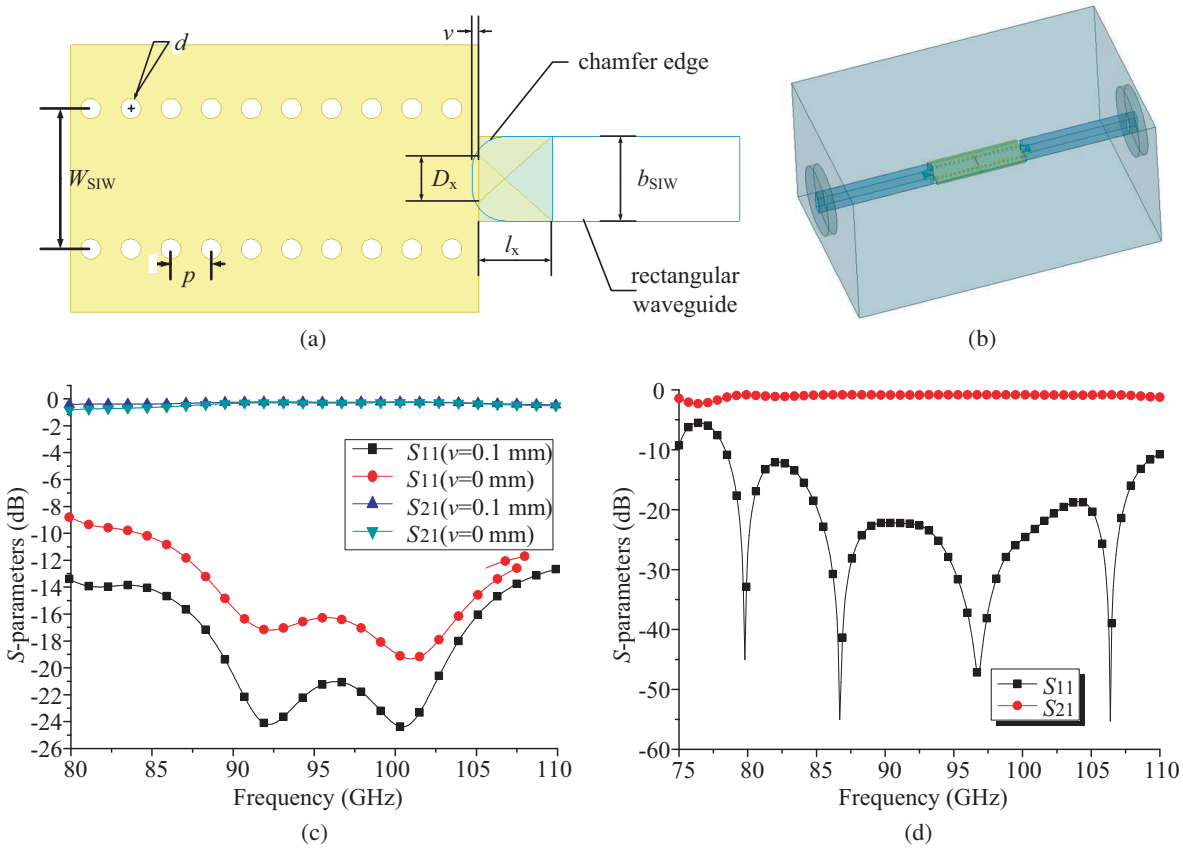

Figure 6. Designed back-to-back fin-line SIW-RW transition. (a) Modification of the transition, (b) back-to-back fin-line SIW-RW transition, (c) numerical results of the modified transition, and (d) numerical results of the back-to-back fin-line SIW-RW transition.

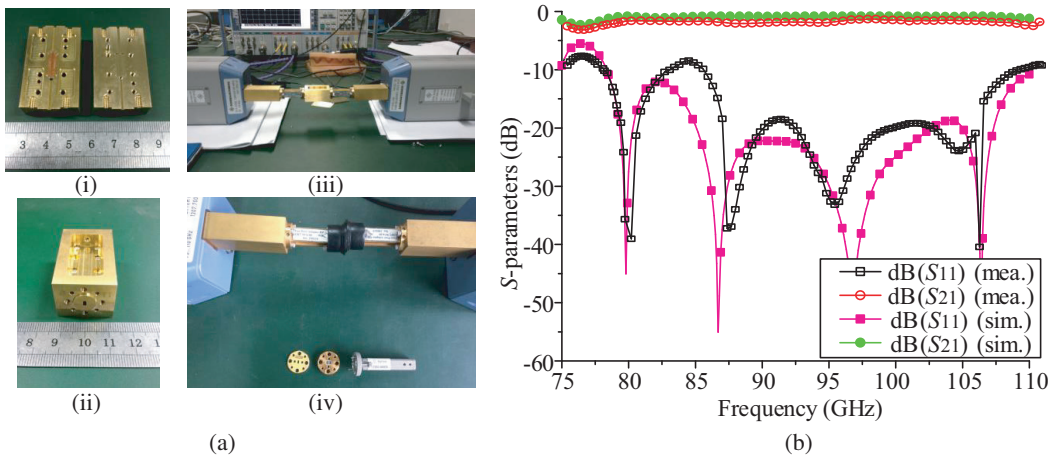

Figure 7. Experimental demonstrations of the fin-line SIW-RW transition. (a) Fabricated sample, measurement setup, and TRL calibration Kit, and (b) measured results of the transition.

Fig. 6(b) to check the performance of the antipodal fin-line SIW-RW transition with the structural parameters obtained before, and the simulated results are shown in Fig. 6(d). It can be seen that the overall return loss is larger 15 dB and inserting loss smaller than 1.5 dB in the frequency range of 85 GHz to 107 GHz.

Then, we fabricate the real antipodal fin-line SIW-RW transition to demonstrate the performance experimentally. From Fig. 6(b), this device is composed of the SIW and metallic rectangular waveguide. So the SIW is fabricated through standard printed circuit board technique on a 0.508 mm Rogers RT/duriod 5880 dielectric substrate with cooper thickness of 0.017 mm. The fabricated SIW can be found in Figs. 7(a)–(i). Then the SIW is fixed tightly by using the fabricated metallic rectangular waveguide with flanges as shown in Figs. 7(a)–(ii). Lastly, the assembled transition is connected to the R&S ZVA67 vector network analyzer (see Figs. 7(a)–(iii)) with frequency converters which can cover the whole W band. The thru-reflect-line (TRL) calibration procedure [33] is performed to eliminate the system errors during measurements, and the used TRL Kit can be found in Figs. 7(a)–(iv).

The measured transmission and reflection properties of the antipodal fin-line SIW-RW transition are shown in Fig. 7(b). It is seen that the measured inserting loss is 1.9 dB $\pm$ 0.3 dB, and return loss is larger than 15 dB in the frequency range of 86.4 GHz–106.1 GHz. Comparing the measured results with the numerical results at the same plot as show in Fig. 7(b) shows that the measured performance (inserting loss) is slightly worse than the corresponding numerical result. This mainly comes from the fabrication tolerance, assembling process, and measurement process.

4. EXPERIMENTALLY DEMONSTRATION OF THE SIW FOUR-WAY POWER COMBINER/DIVIDER

Lastly, after we have obtained the four-way longitudinal-slot coupling structure and the antipodal fin-line SIW-RW transition, the SIW four-way power combiner/divider is designed based on the above two components. Here we also design the back-to-back configuration for the convenience of measurement. As shown in Fig. 8(a), it consists of the back-to-back four-way longitudinal-slot coupling structure placed in the center and two antipodal fin-line SIW-RW transitions placed on the two terminals of the coupling structure. Then two measurement rectangular waveguides are connected to the output of the two transitions.

We do the numerical simulation again to double check the design based on the above obtained structural parameters. As shown in Fig. 8(b), the inserting loss is about 3.65 dB, and the return loss is larger than 15 dB in the frequency range of 91.95 GHz–93.5 GHz. Compared to the numerical results (see Fig. 4(f)) for the four-way longitudinal-slot coupling structure only, the performances of the final design have slight deteriorations. This is because of the added two antipodal fin-line SIW-RW transitions.

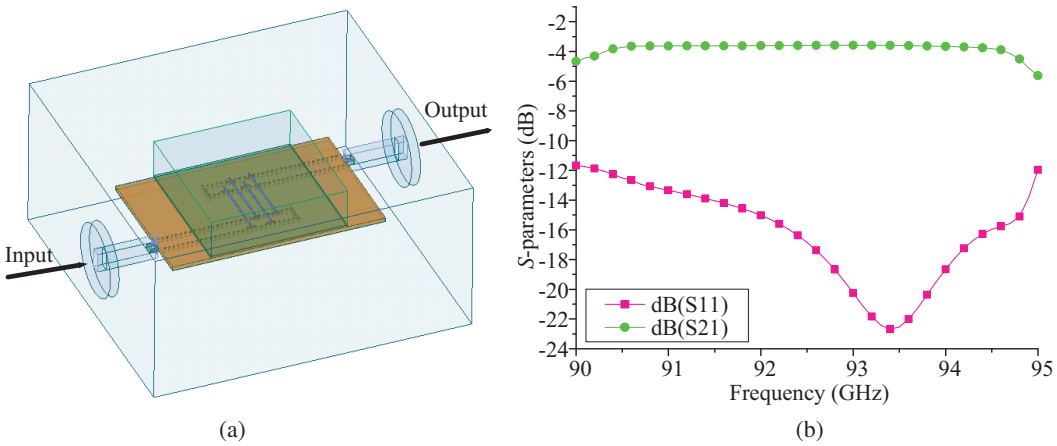

Figure 8. Numerical demonstrations of the SIW power combiner/divider. (a) Designed SIW power combiner/divider, and (b) numerical results of the SIW power combiner/divider.

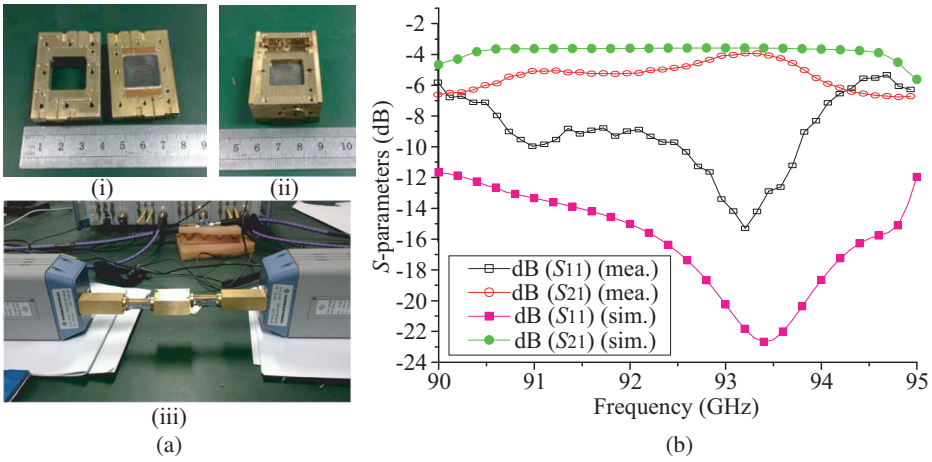

Figure 9. Experimental demonstrations of the SIW power combiner/divider. (a) Fabricated sample and the measurement setup, and (b) measured results of the SIW power combiner/divider.

Then, we directly fabricate the full SIW four-way power combiner/divider. Also, the SIW layer and microstrip layer are fabricated through standard printed circuit board technique on the 0.508 mm Rogers RT/duriod 5880 dielectric substrate with cooper thickness of 0.017 mm. The fabricated SIW and microstrip are overlapped (see Figs. 9(a)–(i)), assembled, and fixed tightly by using the fabricated metallic rectangular waveguide with flanges as shown in Figs. 9(a)–(ii). Lastly, the assembled combiner/divider is connected to the R&S ZVA67 vector network analyzer (see Figs. 9(a)–(iii)) with frequency converters which can cover the whole W band. The TRL calibration procedure is performed as well to eliminate the system errors during measurements.

The real measured results are shown in Fig. 9(b), and the corresponding numerical results are reproduced here for comparisons as well. It can be seen that the measured inserting loss is about 3.9 dB, and the return loss is larger than 10 dB in the range of 92.8 GHz–93.8 GHz. The minimum inserting loss is 3.75 dB located at 93.4 GHz with return loss of 15.1 dB. Compared with the corresponding numerical results as shown in Fig. 9(b), the measured results are worse for all the frequency range. Specially, the inserting loss and return loss at low and high frequency ranges are deteriorated quickly. As mentioned before, the main reasons are the fabrication tolerance, assembling process, and measurement process. The first problem can be solved by using higher quality fabrication process such as lithography technique, and the last two problems can be further reduced by carefully assembling the devices and performing the experiments and calibrations.

5. CONCLUSION

In this paper, we experimentally/numerically propose and demonstrate a novel W-band substrate integrated waveguide (SIW) power combiner/divider based on the antipodal fin-line SIW-rectangular waveguide (SIW-RW) transition and longitudinal slot coupling techniques. The antipodal fin-line SIW-RW transition demonstrates that the return loss is larger than 15 dB and inserting loss less than 2 dB in the operating frequency band of 86.4 GHz–106.1 GHz. By combining the antipodal fin-line SIW-RW into the four-way longitudinal-slot SIW coupling structure, the back-to-back power dividing/combining system is achieved, which can operate at the frequency band of 92.8 GHz–93.8 GHz with return loss more than 10 dB and insertion loss less than 3.9 dB. This design can be easily used in future for the spatial power amplifier applications.

ACKNOWLEDGMENT

This work was supported in part by the National Natural Science Foundation of China (Grant Nos. 61371047, 61601093), the Guangdong Provincial Science and Technology Planning Program (Industrial High-Tech Field) of China under project contract No. 2016A010101036, and by Sichuan Provincial Science and Technology Planning Program (Technology Supporting Plan) of China under project contracts No. 2016GZ0061.

REFERENCES

1. Chang, K. and C. Sun, "Millimeter-wave power-combining techniques," *IEEE Trans. Microwave Theory and Techniques*, Vol. 31, 91–107, 1983.
2. Shiffler, D., J. Nation, and G. S. Kerslick, "A high-power, traveling wave tube amplifier," *IEEE Trans. Plasma Science*, Vol. 18, 546–552, 1990.
3. Yoo, C. and Q. Huang, "A common-gate switched 0.9-W Class-E power amplifier with 41% PAE in 0.25-μm CMOS," *IEEE Journal of Solid-State Circuits*, Vol. 36, 823–830, 2001.
4. Jia, P., L. Y. Chen, A. Alexanian, and R. York, "Broad-band high-power amplifier using spatial power-combining technique," *IEEE Trans. Microwave Theory and Techniques*, Vol. 51, 2469–2475, 2003.
5. Wang, F., D. F. Kimball, J. D. Popp, A. H. Yang, D. Y. Lie, P. M. Asbeck, and L. E. Larson, "An improved power-added efficiency 19-dBm hybrid envelope elimination and restoration power amplifier for 802.11 g WLAN applications," *IEEE Trans. Microwave Theory and Techniques*, Vol. 54, 4086–4099, 2006.
6. He, S. and K. Liu, "On the possibility of a perfect power combiner," *Progress In Electromagnetics Research*, Vol. 158, 1–6, 2017.
7. Bashirullah, R. and A. Mortazawi, "A slotted-waveguide power amplifier for spatial power-combining applications," *IEEE Trans. Microwave Theory and Techniques*, Vol. 48, 1142–1147, 2000.
8. Song, K. and Q. Xue, "Planar probe coaxial-waveguide power combiner/divider," *IEEE Trans. Microwave Theory and Techniques*, Vol. 57, 2761–2767, 2009.
9. Wu, K., "Integration and interconnect techniques of planar and non-planar structures for microwave and millimeter-wave circuits-current status and future trend," *Asia-Pacific Microwave Conference*, 411–416, 2001.
10. Abdolhamidi, M. and M. Shahabadi, "X-band substrate integrated waveguide amplifier," *IEEE Microwave and Wireless Components Letters*, Vol. 18, 815–817, 2008.
11. Germain. S., D. Deslandes, and K. Wu, "Development of substrate integrated waveguide power dividers," *Canadian Conference on Electrical and Computer Engineering*, Vol. 3, 1921–1924, 2003.
12. Hao, Z., W. Hong, H. Li, H. Zhang, and K. Wu, "Multiway broadband substrate integrated waveguide (SIW) power divider," *IEEE Antennas and Propagation Society International Symposium*, 639–642, 2005.

13. Liu, B., W. Hong, L. Tian, H. B. Zhu, W. Jiang, and K. Wu, "Half mode substrate integrated waveguide HMSIW multi-way power divider," *Asia-Pacific Microwave Conference*, 2006.
14. Jin, H. and G. Wen, "A novel four-way Ka-band spatial power combiner based on HMSIW," *IEEE Microwave and Wireless Components Letters*, Vol. 18, 515–517, 2008.
15. Yang, N., C. Caloz, and K. Wu, "Substrate integrated waveguide power divider based on multimode interference imaging," *IEEE MTT-S International Microwave Symposium Digest*, 883–886, 2008.
16. Song, K., Y. Fan, and Y. Zhang, "Eight-way substrate integrated waveguide power divider with low insertion loss," *IEEE Trans. Microwave Theory and Techniques*, Vol. 56, 1473–1477, 2008.
17. Eom, D. S., J. Byun, and H. Y. Lee, "Multilayer substrate integrated waveguide four-way out-of-phase power divider," *IEEE Trans. Microwave Theory and Techniques*, Vol. 57, 3469–3476, 2009.
18. Mohammadi, P. and S. Demir, "Two layers substrate integrated waveguide power divider," *2011 XXXth URSI General Assembly and Scientific Symposium*, 2011.
19. Lee, D. M., Y. J. An, and J. G. Yook, "An eight-way radial switch based on SIW power divider," *Journal of Electromagnetic Engineering and Science*, Vol. 12, 216–222, 2012.
20. Song, K., F. Zhang, F. Chen, and Y. Fan, "Wideband millimetre-wave four-way spatial power combiner based on multilayer SIW," *Journal of Electromagnetic Waves and Applications*, Vol. 27, No. 13, 1715–1719, 2013.
21. Zheng, P., P. Zhou, W. H. Yu, H. J. Sun, X. Lv, and H. Deng, "W-band power divider based on H-plane slot waveguide bridge," *International Conference on Microwave and Millimeter Wave Technology (ICMMT)*, 1–4, 2012.
22. Zhao, X., X. Q. Xie, L. Zhou, and Y. L. Wu, "Four-way power divider/combiner based on waveguide microstrip structure in W-band," *International Conference on Microwave and Millimeter Wave Technology (ICMMT)*, 1–4, 2012.
23. Ma, R., M. Luo, H. Sun, Z. Li, and P. Zheng, "Design and simulation of a W-band two-way power divider based on substrate integrated waveguide," *IEEE International Conference on Microwave Technology and Computational Electromagnetics (ICMTCE)*, 100–102, 2013.
24. Li, J., Y. Chu, and J. Xu, "A novel W-band solid-state power divider/combiner network based on waveguide microstrip structure," *2014 IEEE International Conference on Communication Problem-Solving (ICCP)*, 266–268, 2014.
25. Chen, K., B. Yan, and R. Xu, "A novel W-band ultra-wideband substrate integrated waveguide (SIW) T-junction power divider," *Proceedings of International Symposium on Signals, Systems and Electronics (ISSSE)*, 1–3, 2010.
26. Yee, H. Y., "Impedance of a narrow longitudinal shunt slot in a slotted waveguide array," *IEEE Trans. Antennas and Propagation*, Vol. 22, 589–592, 1974.
27. Oliner, A. A., "The impedance properties of narrow radiating slots in the broad face of rectangular waveguide," *IRE Trans. Antennas Propagation Parts I and II*, Vol. 5, 4–20, 1957.
28. Josefsson, L. G., "Analysis of longitudinal slots in rectangular waveguide," *IEEE Trans. Antennas and Propagation*, Vol. 35, 1531–1537, 1987.
29. Jiang, X., L. Liu, S. C. Ortiz, R. Bashirullah, and A. Mortazawi, "A Ka-band power amplifier based on a low-profile slotted-waveguide power-combining/dividing circuit," *IEEE Trans. Microwave Theory and Techniques*, Vol. 51, 144–146, 2000.
30. Che, W., K. Deng, D. Wang, and Y. L. Chow, "Analytical equivalence between substrate-integrated waveguide and rectangular waveguide," *IET Microwaves, Antennas & Propagation*, Vol. 2, 35–41, 2008.
31. Rebollo, A., R. Gonzalo, and I. Ederra, "An inline microstrip-to-waveguide transition operating in the full W-band," *J. Infrared Milli. Terahz. Waves*, Vol. 36, 734–744, 2015.
32. Van Heuven, J. H. C., "A new integrated waveguide-microstrip transition," *IEEE Trans. Microwave Theory and Techniques*, Vol. 24, 144–147, 1976.
33. Engen, G. F. and C. A. Hoer, "Thru-reflect-line: An improved technique for calibration the dual six-port automatic network analyser," *IEEE Trans. Microwave Theory Techniques*, Vol. 27, 987–993, 1979.